Progress in Organic Coatings 183 (2023) 107716

Contents lists available at ScienceDirect

Progress in Organic Coatings

journal homepage: www.elsevier.com/locate/porgcoat

Corrosion inhibition performance of developed epoxy coatings containing carbon nanocapsules loaded with diethylenetriamine

Norhan Ashraf Ismail [a,b], R.A. Shakoor [a,*], Ramazan Kahraman [b,*]

[a] Center for Advanced Materials, Qatar University, Doha 2713, Qatar
[b] Department of Chemical Engineering, College of Engineering, Qatar University, Doha 2713, Qatar

ARTICLE INFO

Keywords:
Hollow carbon spheres
DETA
Epoxy coating
Corrosion inhibition
Nanocapsules
Mesoporous structure

ABSTRACT

In recent years, hollow structured nanomaterials owe high attention to research, especially when applied to organic coatings due to their high surface area, loading capacity, and flexible shape and structure. Towards this direction, mesoporous hollow carbon nanospheres (MPHS) have been synthesized using the self-assembly method with an average diameter of 280 nm using silica particles as a hard template. The etching of the silica cores was carried out using alkaline etching with NaOH which effectively removed the cores as confirmed by the EDX and FTIR. The MPHS has BET surface area, pore volume, and pore radius of 830.8 m^2/g, 1.1 cc/g, and 3.4 nm respectively which support the loading of diethylenetriamine (DETA). The DETA acts as a corrosion inhibitor, surface modifier, and hardener loaded into MPHS with a high loading rate (44 %) to develop MPHS@ DETA. 3 wt% of the MPHS@ DETA was blended with an epoxy coating (MPHS@ DETA-EP) as an anti-corrosion pigment and then the properties of the developed epoxy coatings were systematically characterized. The developed MPHS@ DETA-EP shows excellent anti-corrosion behavior after continuous exposure to corrosive media for 40 days making the coating suitable for several industrial applications.

1. Introduction

As there is always a probability of metal attack by continuous exposure to harsh environmental factors. Thus, the organic coating application is a potential strategy to protect metallic materials against corrosion. Epoxy is one of the most effectively used materials for coating purposes due to its high chemical stability, excellent mechanical properties, and good adhesion. On the other hand, organic coatings can be permeable and pass the corrosive ions through their micropores by the continuous exposure of the coating to a corrosive environment. As result, a corrosion product will be formed on the steel surface which will cause a failure of the coating's protective property. Hence, nanocomposite coatings are considered to be an effective solution that compensates for the disadvantages of organic coatings by reinforcing nanocontainers that act as fillers by narrowing the gaps in the microstructure of the coating which minimizes the passage of the corrosive ions and enhancing the corrosion resistance of the coatings [1]. Moreover, the coating properties could be further improved by the incorporation of a corrosion inhibitor hosted by the nanocontainers. Recently, nanocontainers with mesoporous structures become an interesting topic that attracted the attention of several researchers [2–4]. Furthermore, hollow mesoporous carbon nanomaterials have proven their good performance in different fields due to their high specific surface area, high aspect ratio, high thermal stability, good electron transport capability, flexible shape and structure, and large vacancy for mass loading [5]. Based on the structure, the hollow carbon nanomaterials could be presented as hollow nanofibers, nanocages, bowl-like, MOF-based, spheres with hard templates, or spheres without templates [6]. The hollow structure could be achieved using three preparation methods such as soft, hard, and self-templating combined with several techniques such as etching, nano casting, chemical vapor deposition, layer-by-layer assembly, spray pyrolysis, etc. [7]. One of the hollow mesoporous carbon nanomaterials that have proven its effectiveness in the last few years is the hollow mesoporous carbon spheres [8–10]. The hollow mesoporous carbon spheres can be without hybrid materials such as single-shell, double-shell, multi-shell, and yolk-shell or can be hybrid materials based such as with coating, supporting, sandwich, multi-yolk, and single-yolk [7]. The hollow mesoporous carbon spheres are known as carbon capsules because of their hollow structure with thin carbon shells. The size of hollow mesoporous carbon spheres can vary from millimeter to nanometer size. Recently, the hollow carbon spheres have been applied in several fields such as batteries [11,12], dyes removal

* Corresponding authors.
E-mail addresses: shakoor@qu.edu.qa (R.A. Shakoor), ramazank@qu.edu.qa (R. Kahraman).

https://doi.org/10.1016/j.porgcoat.2023.107716
Received 15 January 2023; Received in revised form 8 May 2023; Accepted 29 May 2023
Available online 9 June 2023

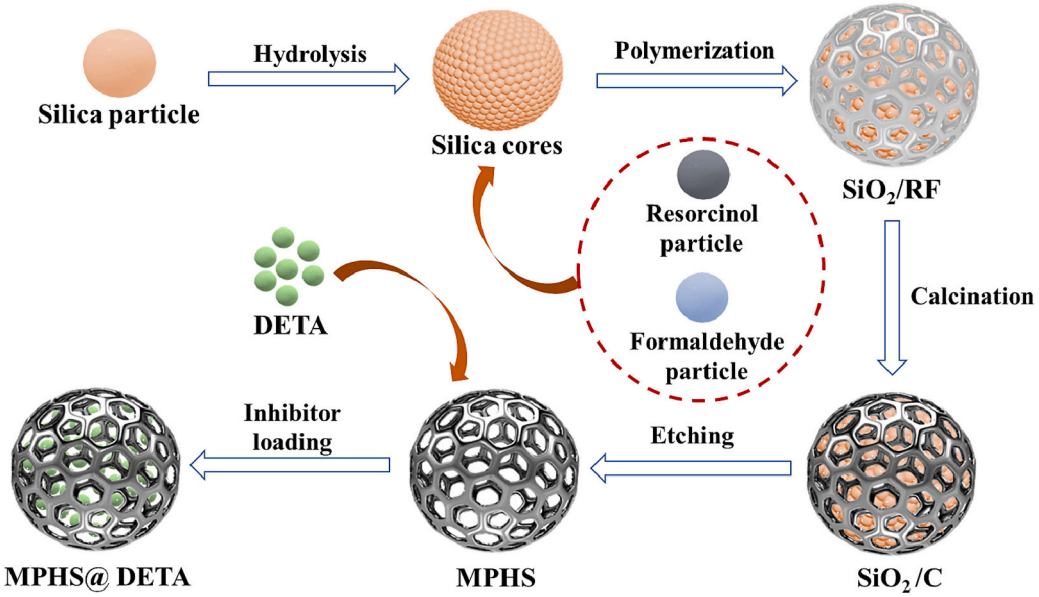

Fig. 1. Scheme for the structure of the MPHS@ DETA with the synthesis steps

[13], adsorption [14], energy storage [15,16], and others due to their easily tunable particle size, high encapsulation capability, outstanding thermal and chemical stability, and surface functionality. As stated recently in the literature, the synthesis and application of hollow mesoporous carbon spheres as an organic host/reservoir have been reported in a few research. Haddadi et al. [17] synthesized carbon hollow spheres (CHSs) using the silica templating method and encapsulated them with 2-mercaptobenzimidazole (MBI) inhibitor to study their corrosion inhibition performance by exposure ta o saline environment. The study highlighted that the released MBI has been absorbed onto the surface of the steel samples after 24 h immersion in the MBI-doped CHSs extract solution. Behgam et al. [18] developed Zn@HCS nanoparticles by doping zinc cations into hollow carbon spheres to evaluate the corrosion inhibition effect of released zinc cations in saline solution on bare mild steel samples. The released zinc cations are effectively deposited as zinc hydroxide/oxide over the steel surface, forming an inhibitive film. Several updated research further examined the behavior of hollow carbon spheres by the application in epoxy coatings for corrosion protection. Haddadi et al. [19] synthesized hollow carbon spheres and employed them in epoxy and polyamine as the film-forming agent which showed an enhancement in the self-healing properties. In another research [20], the hollow carbon spheres have been loaded with walnut extract as a green corrosion inhibitor in epoxy coating. The developed epoxy coating showed an improvement of ~1450 % in the corrosion protection behavior compared with the blank coating. Moreover, in another work [21], carbon nanospheres with dual-encapsulated epoxy/polyamine were dispersed uniformly in the epoxy resin at different concentrations (2, 5, and 10 wt%). It was noticed that the carbon nanospheres enhanced the barrier properties, corrosion protection performance the mechanical properties of the epoxy coating. In addition, the epoxy coating containing the highest concentration of carbon nanospheres has higher scratch hardness. Hao et al. [22] developed epoxy coating reinforced with mesoporous polyaniline (PANI) hollow spheres loaded with benzotriazole (BTA) corrosion inhibitor (MPHS@BTA) with 27 % loading using mesoporous carbons hollow spheres and PS_{100}-b-PEO_{114} as a hard template and soft template respectively. The developed epoxy coating provided high corrosion resistance due to the passivation function of PANI and the corrosion inhibition effect of BTA. On the other hand, no research has reported the loading of a multifunctional inhibitor (especially from the amines family) into the mesoporous hollow carbon spheres and studied the effect of this inhibitor loading on the coating performance. The corrosion inhibition properties of DETA have been studied in a chloride solution saturated with CO_2 [23] and in a hydrochloric acid solution [24]. However, the phenomenon has not been explored for DETA when loaded into a nanoreservoir, employed in the polymeric coating, and exposed to neutral media. Moreover, the high loading rate reported herein offered an enhanced and prolonged anti-corrosion behavior for the developed coating. In the presented work, the mesoporous hollow carbon spheres (MPHS) have been synthesized by the self-assembly method using tetraethyl orthosilicate (TEOS) as a silica source to obtain the in situ SiO_2 particles as hard templates by the hydrolysis, resorcinol-formaldehyde resin as a carbon source to be deposited on the SiO_2 cores using polymerization process followed by carbonization at high temperature and alkaline eco-friendly etching using NaOH. Then, the obtained MPHS was loaded with diethylenetriamine (DETA) (MPHS@ DETA) which acts as a corrosion inhibitor. Besides the main function of DETA as a corrosion inhibitor, it acts as a hardener for the epoxy which increases the hardness and strength of the coating. Moreover, as DETA contains two primary amines at both sides of its structure and a secondary amine between two ethylene groups, it modified the surface of the MPHS@ DETA after being loaded into the MPHS by carrying out surface amination modification that helps to have a uniform and controllable loading. Hence, the MPHS@ DETA was dispersed into epoxy resin using a vacuum to obtain MPHS@ DETA-EP. Several characterization analyses have been carried out on the proposed coating (MPHS@ DETA-EP) to evaluate its anti-corrosion ability. It can be concluded that the high storage ability, high thermal stability of the MPHS, and excellent anti-corrosion behavior of MPHS@ DETA-EP make the proposed system suitable for numerous potential applications.

2. Experimental section

2.1. Materials

Formaldehyde (37 wt%), sodium hydroxide, ammonium hydroxide (28 wt%), diethylenetriamine (DETA), tetraethyl orthosilicate (TEOS), Resorcinol, ethanol absolute, epoxy resin (Epon resin 815 C), triethylenetetramine (as an epoxy hardener) and NaCl solution prepared in 3.5 wt% was used as a simulation for the corrosive media. All the chemicals were purchased from Sigma-Aldrich Darmstadt, Germany. Plain carbon steel sheets as substrates obtained from a local source.

2.2. Synthesis of MPHS

Fig. 1 shows the synthesis and loading steps of MPHS. To prepare the hard templates (silica cores), 70 ml of ethanol, 10 ml of H_2O, and 3 ml of ammonium hydroxide were mixed under continuous stirring at room temperature to obtain a homogenous mixture. After that, 3.5 ml of TEOS was added dropwise to the prepared mixture under continuous stirring for 15 min. To deposit the carbon on the prepared silica cores, 0.4 g of resorcinol and 0.6 ml of formaldehyde were added to the prepared solution and left for 24 h (a light brown product will be produced). The obtained product was washed with water and ethanol alternately several times and placed in a vacuum oven at 60 °C overnight to dry. After drying, the product a carbonization process was carried out in an inert atmosphere at 700 °C for 5 h obtaining black powder. The etching process was carried out using 10 ml of 2 M NaOH was added to the powder in a glass bottle and placed in an oven at 70 °C for 12 h. After that, the NaOH solution was poured, and the etching step was repeated. The obtained mixture was left to dry at 90 °C overnight in an oven. The synthesis procedure of MPHS followed the reported process [22].

2.3. Loading of MPHS

The loading of the MPHS with DETA inhibitor was carried out by dispersing MPHS in 30 ml of ethanol containing 10 g of DETA. The stirring of the MPHS and DETA mixture was carried out under a vacuum for 24 h. Then, the obtained product was washed with water and ethanol and centrifugated, then dried in the oven at 60 °C overnight to obtain MPHS@ DETA.

2.4. Preparation of substrates and coatings

The epoxy coatings of the unloaded MPHS (ULMPHS-EP), reference epoxy (blank) and the loaded MPHS (MPHS @DETA-EP) were prepared by separately mixing 3 wt% of the unloaded MPHS and loaded MPHS (MPHS @DETA) respectively with the epoxy and the hardener. The epoxy and epoxy hardener (triethylenetetramine) were mixed in the ratio of 5:1. The total (dry film thickness) DFT of both coatings is ~400 μm including a 100 μm pre-layer of blank epoxy and 300 μm of MPHS@DETA-EP layer. The blank epoxy pre-layer was added directly to the steel before adding the MPHS@DETA-EP layer to avoid direct contact of carbon with the steel. The procedure of substrates and coatings preparation was proposed in detail in our previous work [25].

2.5. Characterization

The equipment and specifications of the characterization tests used in the current study were explained in detail in our previous work [25,26]. Moreover, the DC (direct current) potentiodynamic polarization experiments were carried out to observe the anti-corrosion behavior of the bare carbon steel substrates in the presence and absence of a DETA inhibitor. The test was done in two stages, the first stage using 3.5 wt% NaCl as a corrosive solution without adding DETA and the second stage with adding DETA with a concentration of 1.00 g/L. The polarization measurements were carried out using a potential range of −0.8 to 1.1 V at a scan rate of 1 mV/s. Corrosion current density (i_{corr}) and corrosion potential (E_{corr}) were determined from the Tafel plot of anodic and cathodic curves using gamry Echem analyst software.

3. Results and discussion

3.1. Morphological analysis of unloaded MPHS and MPHS@ DETA

The detailed morphological structure of the synthesized MPHS during the synthesis process, before and after loading with DETA corrosion inhibitor was characterized by SEM and HRTEM. Furthermore, elemental mapping and EDX have been used to track and quantify the

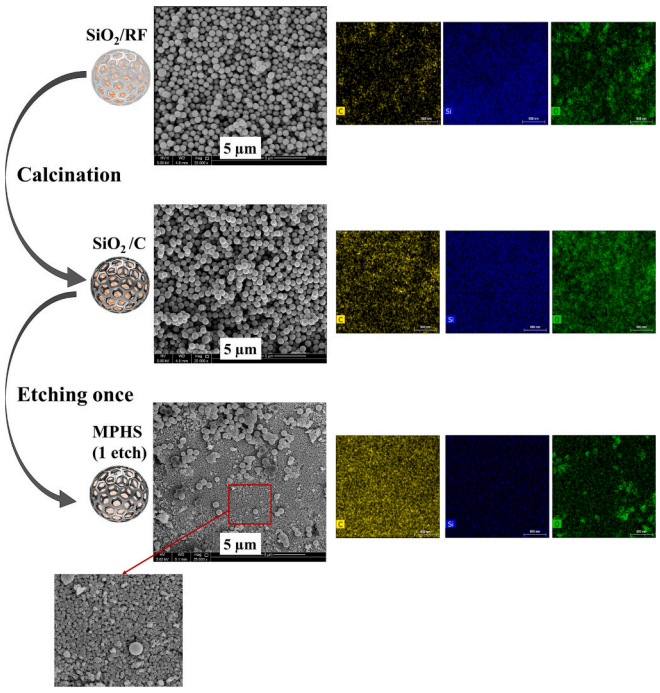

Fig. 2. SEM micrographs with elemental mapping through the MPHS synthesis process (the scale is 5 μm for the micrographs and 800 nm for elemental mapping).

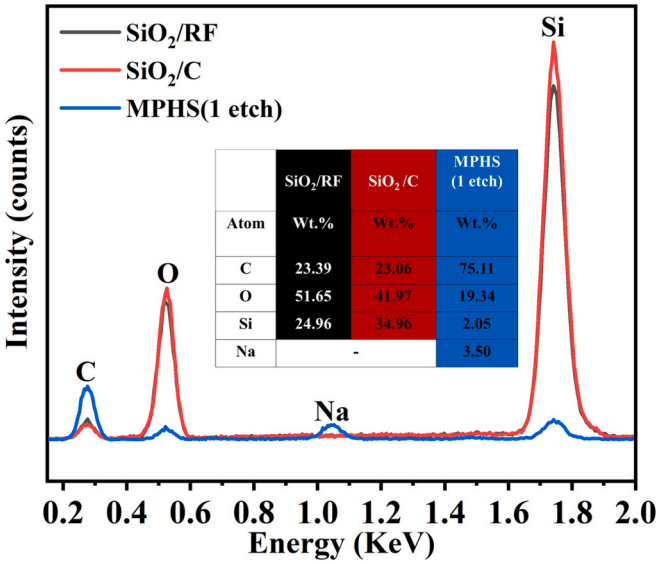

	SiO_2/RF	SiO_2/C	MPHS (1 etch)
Atom	Wt.%	Wt.%	Wt.%
C	23.39	23.06	75.11
O	51.65	41.97	19.34
Si	24.96	34.96	2.05
Na	-		3.50

Fig. 3. EDX of MPHS through the synthesis process.

composition of the MPHS during and after synthesis. Fig. 2 depicts the structure and elemental mapping of the silica templates (SiO_2/RF), the MPHS after the calcination (SiO_2/C), and the MPHS after the etching with NaOH for 1 time. As can be seen in Fig. 2, the spheres presented in a uniform structure and size directly after the polymerization process with a shell of resorcinol and formaldehyde and a high concentration of silicon and oxygen (silica) due to the presence of the dense silica cores as a hard template and a relatively low concentration of carbon due to the casting of the carbon precursors (resorcinol and formaldehyde) on the silica template. The presence of carbon indicates the formation of the main skeleton (shells) of the nanocapsules successfully in the first step (polymerization). After the calcination, the amount of carbon increased due to the conversion of the shell into pure carbon in an inert

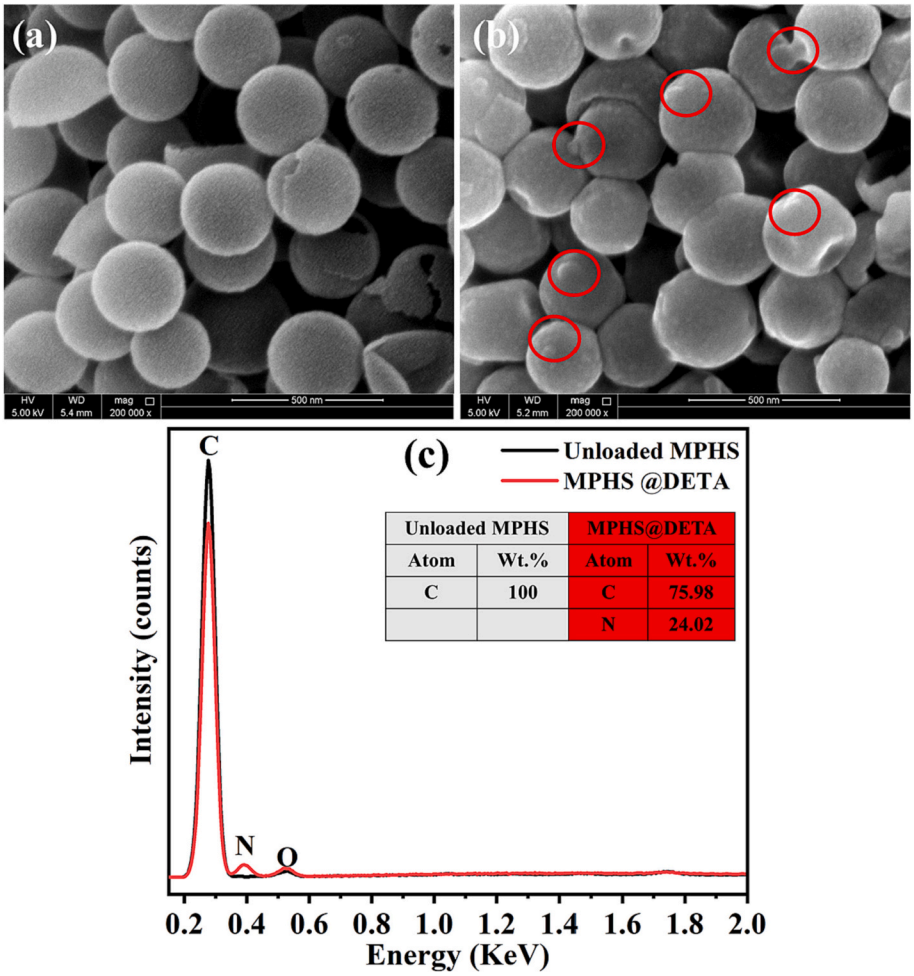

Unloaded MPHS		MPHS@DETA	
Atom	Wt.%	Atom	Wt.%
C	100	C	75.98
		N	24.02

Fig. 4. SEM micrographs for (a) Unloaded MPHS after etching 2 times, (b) MPHS @DETA, and (c) EDX for Unloaded MPHS and MPHS @DETA.

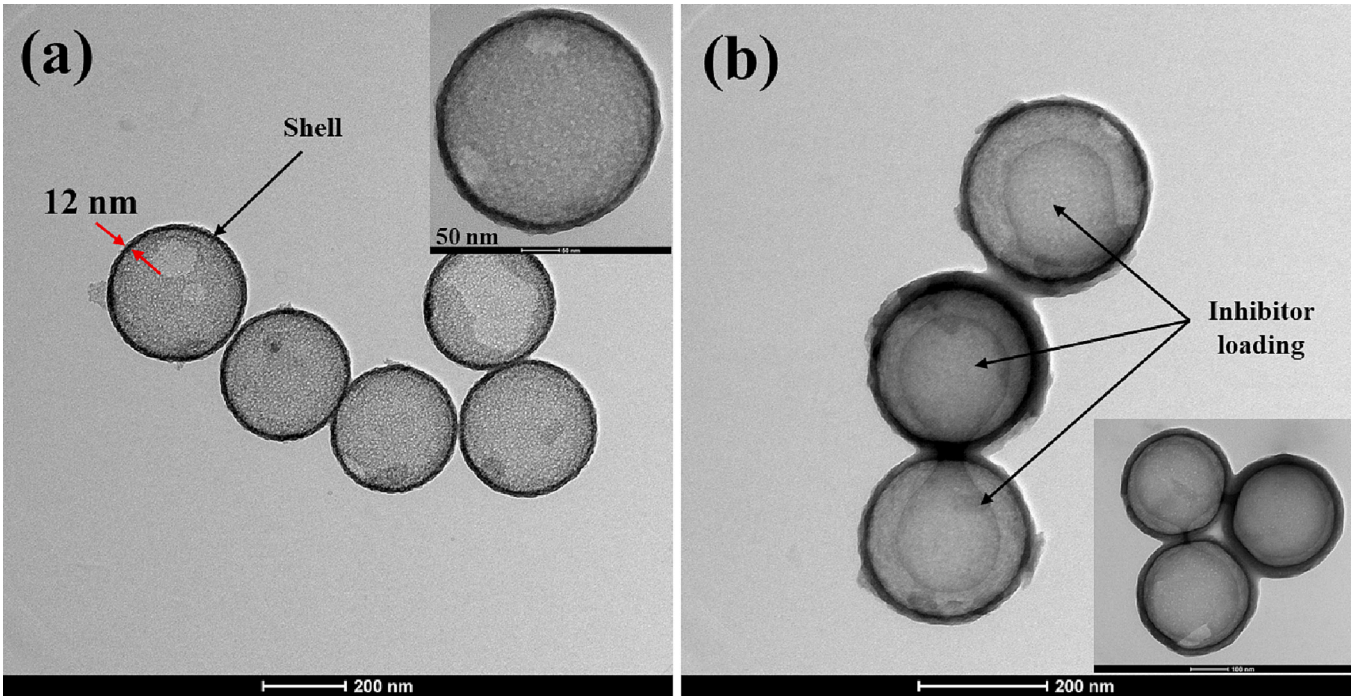

Fig. 5. HRTEM for (a) unloaded MPHS, (b) MPHS @DETA.

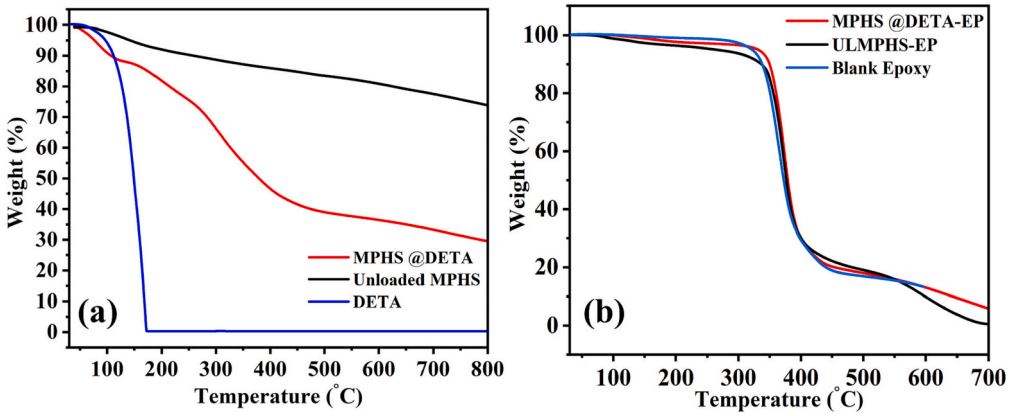

Fig. 6. Thermogravimetric curves of (a) unloaded MPHS, MPHS @DETA, and DETA and (b) coatings.

atmosphere at a high temperature with a similar concentration of silicon and oxygen indicating the completion of the carbonization process and the synthesis of a pure carbon shell. However, after carrying out the NaOH etching once, some of the silica cores have been removed causing a dramatic decrease in the concentration of silicon and oxygen and an increase in the concentration of carbon. Moreover, the spherical morphology of the nanocapsules was preserved with a slight shrinkage detecting their promising stability and flexibility. The findings of the elemental mapping presented in Fig. 2 have been confirmed by the EDX at the same synthesis stages in Fig. 3. Furthermore, the EDX of the MPHS after etching once presented a low intensity of sodium due to the incomplete removal of NaOH from the sample and low intensity of silicon and oxygen which indicated the need for repeating the etching process for a second time. Fig. 4a shows a non-agglomerated and highly uniform spherical shape with a diameter of ~280 nm, which is presented in SEM micrographs of the unloaded MPHS and MPHS@ DETA. Moreover, the cracked particles shown in Fig. 4a prove the hollow structure of the synthesized MPHS carbon nanocapsules by the presence of very thin carbon shells. The loading of DETA was confirmed in Fig. 4b which shows some particles/material inside and on the surface of the spheres (marked in red) and the changing of the texture of the spheres' surface to be more smooth and less rough due to the DETA loading inside the pores. Fig. 4c shows the EDX of the unloaded MPHS (after 2 times of etching) and MPHS@ DETA. The EDX of the unloaded MPHS shows pure carbon with traces of oxygen which are not detectable by the X-rays. However, the EDX of MPHS@ DETA shows the incorporation of nitrogen which indicates the loading of DETA into the unloaded MPHS causing a slight decrease in the carbon amount in the sample. Moreover, the EDX of the unloaded MPHS (after 2 times of etching) and MPHS@ DETA shows no sign of silica presence indicating successful removal of the silica cores using the eco-friendly NaOH etching. In addition, Fig. 5 shows HRTEM images of unloaded MPHS and MPHS @DETA confirming the hollow structure of the synthesized MPHS with large cavities covered by dark shells of carbon with a thickness of ~12 nm. Moreover, a rough surface can be observed for the unloaded MPHS due to the removal of the SiO_2/RF core during the alkaline etching by NaOH which can enhance the functional groups of the spheres by providing more active sites on their surface [27]. The loading of DETA could be further confirmed by the dark color presented in a high amount inside and on the surface of the spheres (Fig. 5b). Fig. 5b shows the hollow spheres with a smoother surface after the loading with DETA which attributed to the surface amination modification carried out to the capsules. The high loading of DETA into the capsules reflecting their high capacity, surface area and porosity which helps to preserve high amount of inhibitor.

3.2. FTIR analysis

The FTIR analysis has been carried out to confirm the successful loading of DETA into the MPHS@ DETA. Fig. S1 shows the FTIR spectrum of unloaded MPHS, DETA, and MPHS@ DETA. For the FTIR spectrum of the unloaded MPHS, a broad peak can be seen at 3017 cm^{-1} indicating the C—H stretching vibration of the MPHS. Moreover, the peaks at 1700 cm^{-1} and 1033 cm^{-1} are attributed to the stretching deformation of C=C and deformation vibration of C—O respectively, which are contained in the MPHS structure. The FTIR spectrum of the unloaded MPHS indicates the successful synthesis of the MPHS carbon nanocapsules using the self-assembly method. Furthermore, the FTIR spectrum of the DETA inhibitor shows dominant peaks at 3250 cm^{-1}, 2900 cm^{-1}, 1600 $cm^{-1,}$ and 829 cm^{-1} associated with the stretching of N—H, C—H, and bending of N—H due to the -NH_2 scissoring mode. In addition, the two peaks at 1125 cm^{-1} and 1055 cm^{-1} are attributed to the C—N due to the secondary and primary amine stretching, sequentially [28]. The dominant peaks in the FTIR spectrum of the unloaded MPHS and DETA can be observed in the FTIR spectrum of MPHS@ DETA which confirmed the successful loading of the DETA inhibitor into the MPHS. Moreover, the absorption band at 1583 cm^{-1} is anticipated to be due to the successful grafting of the amine group (amination surface modification) into the MPHS using DETA which provides an excellent loading [2].

3.3. Thermogravimetric analysis

Fig. 6 represents the thermogravimetric curves of the unloaded MPHS, loaded MPHS (MPHS @DETA), DETA inhibitor, and the epoxy coatings (blank, the unloaded MPHS coating (ULMPHS-EP), and MPHS @DETA-EP). Fig. 6(a) shows the effective loading of DETA into the MPHS (44 % loading). As can be seen, there is a minor weight loss (up to 10 %) in the unloaded MPHS, MPHS @DETA, and DETA inhibitor at about 100 °C because of the moisture/water evaporation [29]. The total weight loss of the unloaded MPHS at 800 °C is ~25 % which is an indication of the high thermal stability of the MPHS (the boiling point of the carbon is 4827 °C). Moreover, it can be observed that the MPHS@ DETA and the DETA inhibitor start degrading at the same temperature (~90 °C) with a similar trend. When the temperature is very close to 200 °C, the DETA inhibitor degrades completely as it has a boiling point of 207 °C. Meanwhile, MPHS@ DETA loses 20 % of its original weight which can be attributed to the degradation of the DETA inhibitor loaded on the surface or in the pores of the MPHS. With a further increase in the temperature (above 207 °C) the MPHS@ DETA witnessed more loss in its weight reaching 30 % of its original weight at 800 °C which indicates a loading of ~45 % of the DETA inhibitor into the MPHS. This decrease in the weight of MPHS@ DETA could be due to the degradation of the DETA loaded inside the MPHS which needs additional heating to be degenerated. Fig. 6(b) shows the thermogravimetric curves of the developed coatings which are blank epoxy, ULMPHS-EP, and MPHS@ DETA-EP. As shown in Fig. 6(b), all the coatings presented a similar TGA

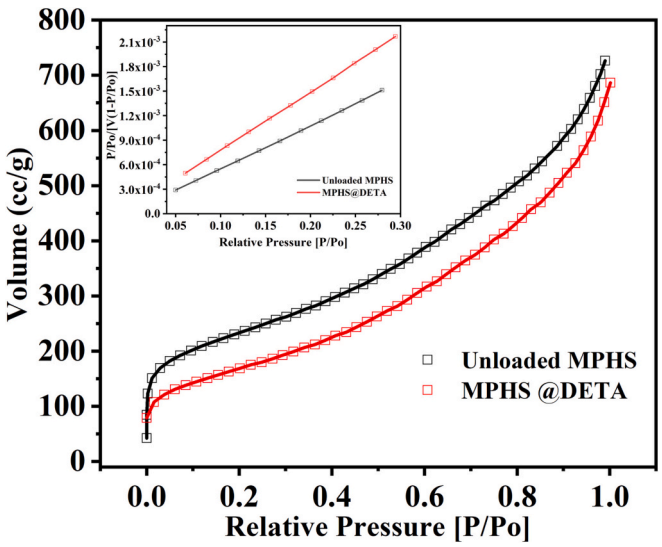

Fig. 7. Nitrogen adsorption isotherm curves of unloaded MPHS and MPHS@ DETA.

trend due to the high quantity of epoxy incorporated in them.

3.4. Brunauer-Emmett-Teller (BET) analysis

Fig. 7 shows the nitrogen adsorption isotherms of unloaded MPHS and MPHS@ DETA which demonstrates the BET surface areas of the unloaded MPHS and MPHS@ DETA with an inset explaining cumulative pore volume. The nitrogen adsorption curves indicate the BET surface area, pore volume, and pore radius of 830.8 m^2/g, 1.1 cc/g, and 3.4 nm for unloaded MPHS respectively. The adsorption on mesoporous solids (such as MPHS) is carried out by multilayer adsorption followed by capillary condensation which results in Type IV isotherm. The main features of Type IV isotherm are the presence of a hysteresis loop incorporated with capillary condensation that is present in the mesopores which limits the nitrogen gas uptake in the high relative pressure (P/P_0) range. In Fig. 7, the capillary condensation step and hysteresis loop can be seen in the P/P_0 range of 0.2 to 0.9 in the nitrogen adsorption curve which is significant for the presence of the mesoporous structure with high pore radius distribution [30]. However, for MPHS@ DETA, the BET surface area, pore volume, and pore diameter decreased to 620.2 m^2/g, 1.1 cc/g, and 2.7 nm respectively, which proved a successful loading of DETA into the MPHS nanoparticles. Furthermore, this drop can be attributed to DETA loading inside and on the pores of the spheres which can cause w partial blockage of the mesoporous channels and a decrease in the surface area. Moreover, the capillary condensation step and hysteresis loop are still can be observed in the MPHS@ DETA nitrogen adsorption curve in the same range of P/P_0 as the unloaded MPHS which is an indication of maintaining the same mesoporous structure after the DETA loading.

3.5. X-ray diffraction (XRD)

The XRD patterns of unloaded MPHS and MPHS@ DETA are shown in Fig. S2. Fig. S2 depicts the intensity of the main peak at ~25° and the secondary peak at ~43° for the loaded and unloaded MPHS which correspond to the planes (002) and (100) respectively, belonging to the carbon. The presence of these peaks confirms the successful formation of the MPHS. Moreover, the XRD patterns show the absence of silica core which implies the successful removal of the silica core by the NaOH eco-friendly etching method. Furthermore, the broadening of the two peaks suggests the low graphitization degree of the MPHS which causes an amorphous structure for the carbon. In addition, the broadening can be an indication of a low range in the structural order. As can be seen, the intensity of the (002) and (100) characteristic peaks slightly increased in the XRD pattern of MPHS@ DETA as the DETA inhibitor is an organic material (containing mainly carbon). The reported results are in agreement with the literature [31–33].

3.6. Electrochemical Impedance Spectroscopy (EIS)

The electrochemical impedance spectroscopy test proceeded to estimate the anti-corrosion behavior of the developed reference coating, ULMPHS-EP and MPHS @DETA-EP by immersion in 3.5 wt% NaCl solution at room temperature for 40 days. Fig. 8 shows the two-time constant electrical circuit which was used in the fitting of EIS experimental data of the two developed coatings which quantify several electrochemical parameters of the coatings. In the applied equivalent electrical circuit, R_s, R_{po}, R_{ct}, CPE1, CPE2, and W are referring to the solution resistance, coating pore resistance, charge transfer resistance at the metal interface, constant phase elements, and Warburg diffusion constant respectively. The constant phase elements (CPE1 and CPE2) are used instead of the capacitance in the equivalent electrical circuit because of the non-ideality of the capacitive behavior of the coatings [34,35]. The constant phase element accounts for the surface roughness and non-homogeneity properties of the analyzed surface because of the passivity (passive layer formation) caused by the species adsorbed on the metal surface [36]. In addition, CPE expresses the nonideal capacitor behavior of the analyzed coatings due to the non-uniform distribution of the applied current over the coating surface [37].

Bode and phase angle plots determine the anti-corrosion mechanism of the developed coatings as represented in Fig. 9. Generally, the difference in the phase angle and impedance plots at the low-frequency range is an indication of the anti-corrosive behavior of the coatings [38]. The change in the impedance values in the low-frequency range of the bode plot determines the barrier property of the developed coatings. Generally speaking, the increase in impedance value at the low-frequency range reveals a higher anti-corrosion ability of the coating. Fig. 9 shows a variation in the impedance values of the ULMPHS-EP and MPHS @DETA-EP. Fig. 9a shows the bode and phase angle graphs of the

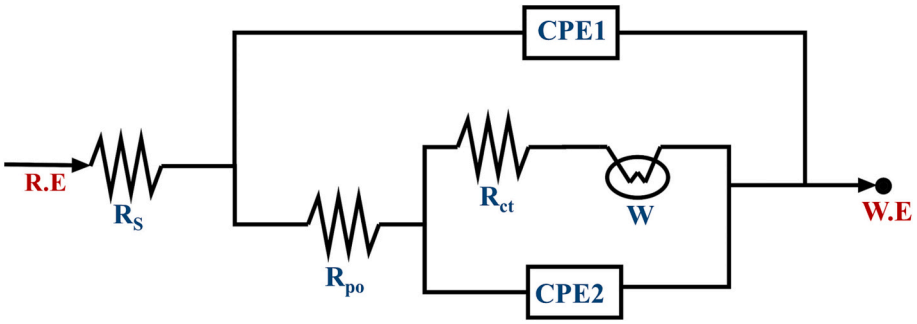

Fig. 8. Equivalent electrical circuit used for EIS fitting for ULMPHS-EP and MPHS @DETA-EP.

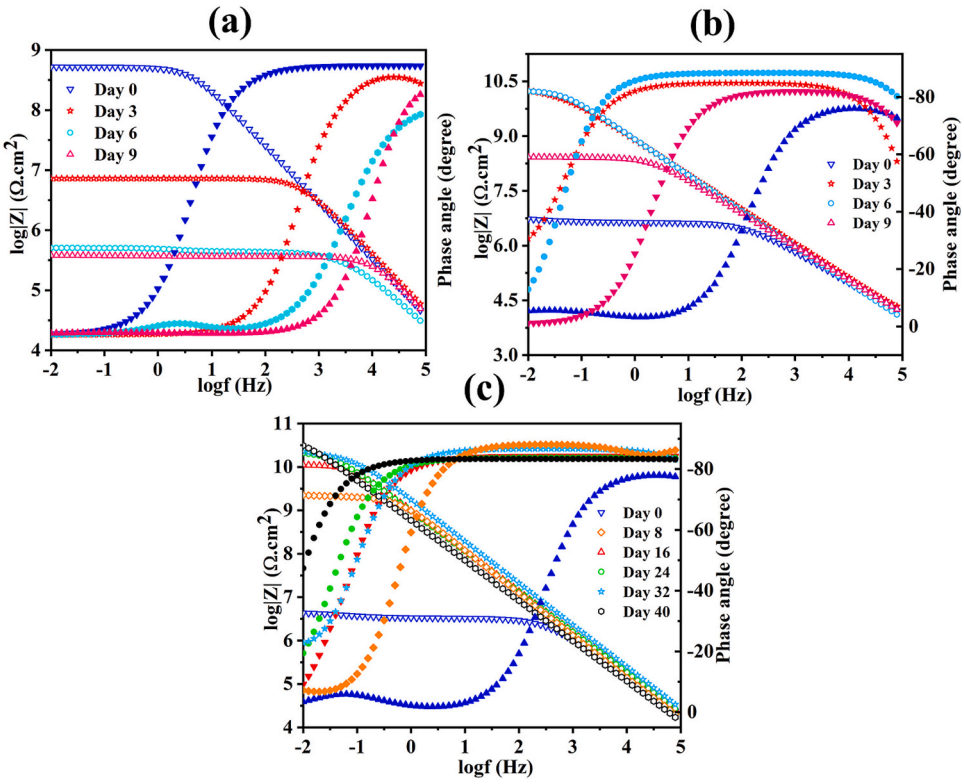

Fig. 9. Bode and phase angle plots for (a) reference epoxy (blank), (b) ULMPHS-EP and (c) MPHS @DETA-EP.

blank epoxy coating. In the high-frequency range, the impedance results show capacitive behavior. However, in the low-frequency range, the charge transfer resistance is 6.51 × 10^6 Ω•cm^2 directly after the immersion, which started decreasing gradually for the successive duration of immersion for nine days until 1.99 × 10^5 Ω•cm^2. This reduction confirms the initiation of the corrosion activity at the interface between the coating and the steel due to the absence of an inhibitor, which can postpone the corrosion propagation. Moreover, the increase of the phase angle of the reference coating to nearly 0° after 9 days of immersion (at the low-frequency range) can be a further confirmation of the reaching of the corrosion ions to the steel surface. In Fig. 9b, a continuous increase in the impedance values can be observed for ULMPHS-EP after the first 6 days of the immersion time from 5.2 × 10^6 Ω.cm^2 to 17.5 × 10^9 Ω.cm^2 indicating that the corrosive ions did not pass the coating to reach the steel surface. However, after 9 days of continuous immersion, the impedance value of the ULMPHS-EP witnessed a significant drop to 261.5 × 10^6 Ω.cm^2, dropped by three orders of magnitude, which was attributed to the passage of the corrosive ions through the coating pores reaching the steel surface. Hence, the protective property becomes low due to the formation of a corrosion product on steel due to the absence of the inhibitor which can delay/prevent the corrosion. The increase of the phase angle of ULMPHS-EP to nearly 0° after 9 days of immersion (at the low-frequency range) can be a confirmation of the reaching of the corrosion ions to the steel surface. Contrary to the ULMPHS-EP anti-corrosion behavior, Fig. 9b shows the phase angle of MPHS @DETA-EP after 40 days of immersion ranging between −20° and -30° which shows a resistor behavior rather than the capacitor behavior [39]. Fig. 9c presents a continuous increase in the impedance values of the MPHS @DETA-EP after 40 days of immersion time from 4.5 × 10^6 Ω.cm^2 to 40.2 × 10^9 Ω.cm^2 which can be attributed to the inhibition effect

Table 1
EIS fitting parameters for ULMPHS-EP and MPHS @DETA-EP.

Coating type	Immersion time (days)	Rpo (Ω.cm^2)	CPE1 (s^n $Ω^{-1}$ cm^{-2})	CPE2 (s^n $Ω^{-1}$ cm^{-2})	Rct (Ω.cm^2)	W
Blank epoxy coating (reference)	0	471.4e6	71.66e-12	110.7e-12	49.21e6	–
	3	5.882e6	73.79e-12	88.17e-12	1.405e6	–
	6	47.18e4	87.7e-12	4.899e-6	38.72e3	–
	9	362.4e3	88.34e-12	49.42e-6	20.89e3	–
Unloaded mesoporous hollow carbon spheres epoxy coating (ULMPHS-EP)	0	4.234e6	604.3e-12	393.8e-9	1.580e4	2.395e-6
	3	1.463e10	270.1e-12	1.66e-12	4.174e4	481.1e-12
	6	17.32e9	159.4e-12	13.46e-9	7.146e5	892.3e-12
	9	2.644e8	180.5e-12	95.29e-9	2.634e5	27.68e-6
Loaded mesoporous hollow carbon spheres with epoxy coating (MPHS @DETA-EP)	0	3.293e6	382.3e-12	1.984e-6	1.220e6	30.60e-3
	8	4.354e7	234.2e-12	51.26e-12	1.789e9	917.1e-9
	16	4.323e7	186.1e-12	1.436e-12	1.974e9	12.40e-9
	24	6.070e9	176.9e-12	85.34e-14	5.606e9	12.07e-9
	32	1.022e10	143.4e-12	1.445e-14	5.473e9	467.9e-12
	40	5.272e10	248.7e-12	88.48e-14	7.032e9	395.1e-9

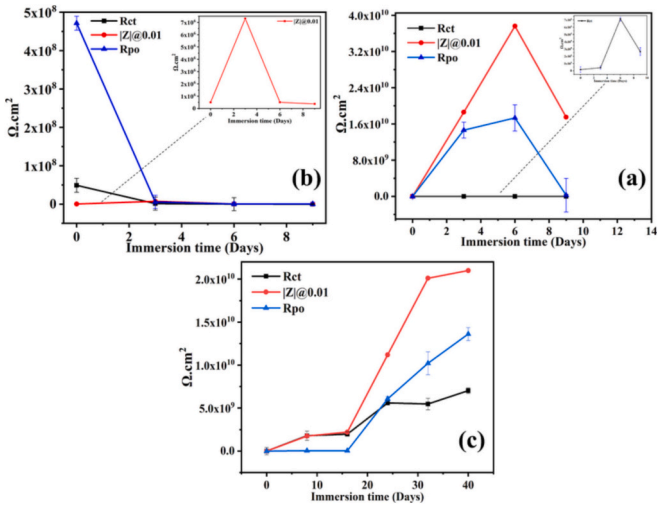

Fig. 10. The trend for Rct, Rpo, and |Z|@0.01 through the complete immersion time for (a) Blank epoxy (reference), (b)ULMPHS-EP and (b) MPHS @DETA-EP coatings.

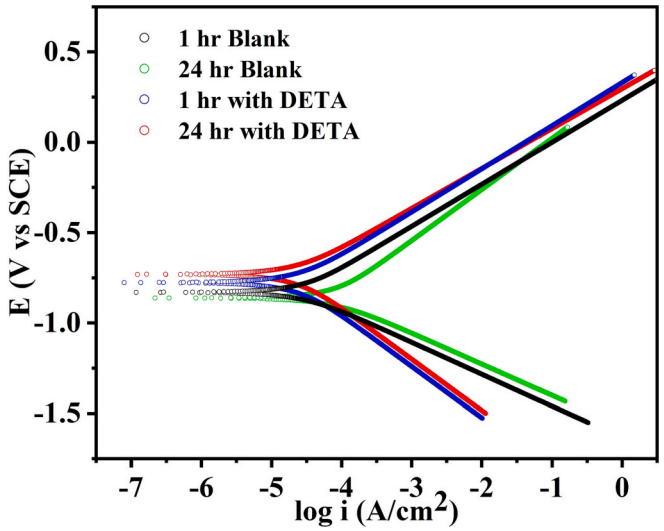

Fig. 11. Tafel plots for uncoated steel with and without DETA presence at different immersion times.

initiation caused by the release of the DETA inhibitor that causes a steel surface prevention against the corrosive ions' penetration. At the high-frequency region, it can be noticed that the phase angle of the coatings ranges from −80° to −89° which is an indication of the excellent durability of the developed epoxy coatings [40].

Furthermore, the parameters used in the fitting of blank epoxy coating, ULMPHS-EP and MPHS @DETA-EP coatings are tabulated in Table 1. Usually, the coating pore resistance (Rpo) and coating constant phase element (CPE1) is used as quantitative tool for the coating performance. CPE1 is used for the characterization of the water absorption of the coating, while Rpo reveals the permeation behavior of the corrosive ions in the coating [41]. Generally, the higher Rpo and lower CPE1 are indications of the high anti-corrosion property of the coating. As can be seen in Table 1, the reference coating shows a dramatic decrease in the Rpo values and increase in CPE1 values in 9 days of immersion which can be attributed to the high corrosive medium permeation. In ULMPHS-EP coating, Rpo increases and CPE1 decreases until 9 days of immersion which reflects a low corrosive medium permeation. The Rpo and CPE1 values increased after 9 days of immersion because of the formation of diffusion channels in the coating in a short time of continuous immersion due to the absence of the inhibitor. However, in MPHS @DETA-EP coating, Rpo increases and CPE1 decreases until 32 days of continuous immersion due to the low permeation of the corrosive media into the coating which reflects the high barrier property of the coating. After 40 days of immersion, CPE1 starts increasing which is anticipated to be due to the complete release of the inhibitor or the reaching of traces of the corrosive ions into the coating-steel interface. Charge transfer resistance (Rct) and constant phase element (CPE2) are used to determine the delamination behavior of the organic coatings from the metallic surfaces. In general, the higher Rct and lower CPE2 indicate a high anti-corrosive performance due to the good adhesion between the organic coating and the metallic surface. As presented in Table 1, in the reference coating, Rct decreases continuously from 49.21 × 10^6 Ω.cm^2 to 20.89 × 10^3 Ω.cm^2 and CPE2 starts increasing after 9 days of immersion which due to the chloride ions penetration through the coating steel interface. In the ULMPHS-EP coating, Rct increases from 1.580 × 10^4 Ω.cm^2 to 7.146 × 10^5 Ω.cm^2 and CPE2 decreases gradually for 6 days of immersion time due to the good adhesion of the coating with the steel and the low diffusion of the corrosive ions through the coating. After 9 days of immersion, Rct decreases to 2.634 × 10^5 Ω.cm^2, and CPE2 increases due to the continuous exposure of the coating into the corrosive media with the absence of the inhibitor which accelerates the diffusion rate of the corrosive ions that causes a poor adhesion of the coating and high water uptake. However, in MPHS @DETA-EP coating, Rct increases continuously from 1.220 × 10^6 Ω.cm^2 to 7.032 × 10^9 Ω.cm^2 and CPE2 starts increasing after prolonged immersion time (40 days) which causes starting of chloride ions penetration through the coating. This trend of the MPHS @DETA-EP is indicating a very slow corrosive media diffusion rate, low water uptake, and excellent adhesion of the coating because of the presence of the DETA inhibitor which protects the steel for a longer time compared with ULMPHS-EP. and prevents direct contact between the coating and the steel. Fig. 10 represents the trend of Rct, Rpo, and the impedance at the low-frequency range (|Z|@0.01) for reference coating, ULMPHS-EP and MPHS @DETA-EP coatings.

In detail, as the coating surface was exposed to the corrosive media (3.5 wt% NaCl solution) which contained oxygen and water for a certain period, a metal deterioration (steel oxidation) started to take place through an anodic reaction. On the other hand, a cathodic reaction has toke place with the decreasing of the inhibitor concentration on the steel surface or when the adsorption rate of the inhibitor is slow. The continuous and direct contact of the corrosive media with the coating caused a change in the localized pH that causes the DETA release from the MPHS nanocapsules. Hence, the water molecules which were occupying the steel surface were replaced by the DETA that was adsorbed on the steel surface, results with an intermediate adsorbed DETA on the steel. As a result, a film of the adsorbed DETA has been formed on the steel surface. The produced inhibitor film plays a role to delay the corrosion activity by blocking the chloride corrosive ions to reach the steel surface.

3.7. Potentiodynamic polarization analysis

The potentiodynamic polarization analysis has been carried out to examine the behavior of the uncoated steel at high impedance levels after proving its high barrier ability using the EIS. In this analysis, two uncoated carbon sheets of steel have been immersed in 3.5 wt% NaCl solution with the presence of DETA and without for 24 h to observe the effect of the DETA inhibitor on the steel. This effect has been studied using direct current polarization and the resulting polarization curves can be seen in Fig. 11. Moreover, Table 2 shows the electrochemical kinetic parameters such as corrosion potential (E_{corr}), corrosion current density (i_{corr}), corrosion rate, and the anodic and cathodic Tafel slopes (βa and βc) which were obtained from the Gamry Echem analyst software. However, the polarization resistance (Rp) has been calculated using the Stern–Geary equation [42] as the following and tabulated in

Table 2
Potentiodynamic polarization parameters obtained from Tafel plots.

Curve	i_{corr} (μAcm^{-2})	E_{corr} (mV)	βa (mV/decade)	βc (mV/decade)	Rp (Ω.cm^2)	θ	Corrosion rate (mpy)	IE (%)
1 h Blank	76.90	−831	242.9	168.3	0.561	–	12.42	–
24 h Blank	215	−862	284.4	171.4	0.216	–	34.76	–
1 h with DETA	66.3	−777	239.4	284.2	0.851	0.691	11.01	69.1
24 h with DETA	63.1	−731	218.4	283.8	0.849	0.706	10.19	70.7

Table 2:

$$R_p = \frac{\beta a\, \beta c}{2.303\, i_{corr}\, (\beta a + \beta c)}$$

Furthermore, the surface coverage (θ) of the DETA on the carbon steel surface can be calculated using the following equation [43] and tabulated in Table 2:

$$\theta = \frac{i'_{corr} - i_{corr}}{i'_{corr}}$$

Where i'_{corr} and i_{corr} are the corrosion current densities measured in the absence and presence of the DETA inhibitor respectively.

It can be observed that the surface coverage increased from 0.691 to 0.706 after 24 h of immersion which indicates the good absorbance of DETA into the steel surface. The Tafel plot of the solution with DETA after 1 h of immersion shows an inhibition effect of DETA which has been indicated by a shift in the corrosion potential (E_{corr}) to −777 mV compared to its value in absence of DETA (−831 mV). As can be seen with the increase in immersion time in the presence of DETA, the corrosion potential witnessed a further shift until reaching −731 mV. This shifting can be attributed to the adsorption of DETA molecules on the steel surface. Moreover, a gradual shift could be observed with the presence of DETA and compared with the absence of DETA towards a lower current density range which proves the reduction in the active sites on the steel due to the linkage of most of them with the inhibitor. In addition, the decrease in the corrosion rate from 34.76 mpy to 10.19 mpy and the increase of the polarization resistance from 0.851 Ω.cm^2 to 0.849 Ω.cm^2 1 h with DETA and after 24 h of immersion in NaCl with DETA highlighting the effect of DETA to protect the steel from the corrosion. Unlike the NaCl with DETA, the potentiodynamic polarization analysis of the NaCl without the DETA inhibitor showed an increase in the corrosion rate from 12.42 mpy to 34.76 mpy and a decrease of the polarization resistance from 0.561 Ω.cm^2 to 0.216 Ω.cm^2 1 h and 24 h in the absence of DETA. The efficiency of the inhibitor can be calculated using the current density by the following equation [44] and tabulated in Table 2:

$$IE(\%) = \left(1 - \frac{i_{corr,b}}{i_{corr,i}}\right) \times 100\%$$

Where $i_{corr,b}$ is the current density in the presence of DETA in μAcm^{-2} and $i_{corr,i}$ is the current density in the absence of DETA in μAcm^{-2}.

The maximum inhibitor efficiency has been calculated after 24 h of continuous immersion in the NaCl solution with DETA as 70.7 %.

4. Conclusion

To sum up, carbon nanocapsules (MPHS) were synthesized using silica cores as a hard template and resorcinol-formaldehyde as a carbon source by the self-assembly technique. A loading and surface amination modification which enhanced the loading into the mesoporous channels of MPHS was carried out on the synthesized MPHS using DETA (MPHS@ DETA). The DETA was loaded into the MPHS with a concentration of ~44 wt% due to its high BET surface area and pore volume. The DETA's corrosion inhibition effect was proved by the potentiodynamic polarization analysis indicating a decrease in the corrosion rate and high inhibitor efficiency reaching 70.7 % compared to a corrosive solution without DETA. Moreover, the MPHS@ DETA was introduced into an epoxy coating to develop MPHS@ DETA-EP which showed excellent anti-corrosion resistance and reached 40.2 × 10^9 Ω.cm^2 after 40 days of exposure to NaCl solution.

CRediT authorship contribution statement

Norhan Ismail: Data curation; Formal analysis; Methodology; Validation; Software; Visualization; Roles/Writing - original draft; Writing - review & editing.

Ramazan Kahraman: Conceptualization; Funding acquisition; Supervision; Project administration.

R. A. Shakoor: Conceptualization; Validation; Funding acquisition; Supervision; Project administration; Resources; Investigation.

Declaration of competing interest

The authors declare that they have no known competing financial interests or personal relationships that could have appeared to influence the work reported in this paper.

Data availability

No data was used for the research described in the article.

Acknowledgment

This publication was made possible by NPRP Grant NPRP 11S–1226-170132 and NPRP 13S-0120-200116 from the Qatar National Research Fund (a member of the Qatar Foundation) and Qatar University internal grant #QUCG-CENG-22/23-461. Statements made herein are solely the responsibility of the authors.

Appendix A. Supplementary data

Supplementary data to this article can be found online at https://doi.org/10.1016/j.porgcoat.2023.107716.

References

[1] M. Rahsepar, F. Mohebbi, H. Hayatdavoudi, Synthesis and characterization of inhibitor-loaded silica nanospheres for active corrosion protection of carbon steel substrate, J. Alloys Compd. 709 (2017) 519–530, https://doi.org/10.1016/j.jallcom.2017.03.104.

[2] H. Chen, C. Yuan, Y. Xuanyu, X. Cheng, A. Elzatahry, A. Alghamdi, J.-C. Su, X. He, Y. Deng, Hollow mesoporous carbon nanospheres loaded with Pt nanoparticles for colorimetric detection of ascorbic acid and glucose, ACS Appl. Nano Mater. 3 (2020), https://doi.org/10.1021/acsanm.0c00638.

[3] W. Han, S. Qiu, J. Chen, X. Zhong, L. Hao, H. Chen, X. Zhou, H. Zhou, One-pot synthesis of mesoporous silica-supported nano-metal oxide composites with enhanced antibacterial properties, Mater. Chem. Phys. (2022), 126618, https://doi.org/10.1016/j.matchemphys.2022.126618.

[4] X. Lu, Z. Xu, Y. Shi, Q. Wang, J. Jia, N. Sun, B. Fang, N. Yuan, J. Ding, Structure engineering of mesoporous MXenes through a general microexplosion assisted exfoliation strategy, J. Alloys Compd. 921 (2022), 166079, https://doi.org/10.1016/j.jallcom.2022.166079.

[5] M. Rahman, M. Ara, M. Alim, M. Uddin, A. Najda, G. Albadrani, A. Sayed, S. Mousa, M. Abdel Daim, Mesoporous carbon: a versatile material for scientific applications, Int. J. Mol. Sci. 29 (2021) 4498, https://doi.org/10.3390/ijms22094498.

[6] F. Liu, Y. Cheng, J. Tan, J. Li, H. Cheng, H. Hu, C. Du, S. Zhao, Y. Yan, M. Liu, Carbon nanomaterials with hollow structures: a mini-review, Front. Chem. 9 (2021), https://doi.org/10.3389/fchem.2021.668336.
[7] T. Liu, L. Zhang, B. Cheng, J. Yu, Hollow carbon spheres and their hybrid nanomaterials in electrochemical energy storage, Adv. Energy Mater. 9 (2019) 1803900, https://doi.org/10.1002/aenm.201803900.
[8] Z. Wei, C. Liu, Y. Zhang, H. Fan, R. Zheng, Z. Wang, Y. Wang, H. Arandiyan, Z. Shao, H. Sun, Y. Liu, Inner wrinkled mesoporous hollow carbon spheres with nanopillars connected to double shells for excellent potassium storage, Carbon N. Y. 200 (2022) 236–246, https://doi.org/10.1016/j.carbon.2022.08.060.
[9] Z. Wang, H. Zhao, K. Chen, H. Li, M. Lan, Sandwich-type electrochemical aptasensor based on hollow mesoporous carbon spheres loaded with porous dendritic Pd@Pt nanoparticles as signal amplifier for ultrasensitive detection of cardiac troponin I, Anal. Chim. Acta 1188 (2021), 339202, https://doi.org/10.1016/j.aca.2021.339202.
[10] S.A. Haddadi, S.A. A. Ramazani, M. Mahdavian, M. Arjmand, Epoxy nanocomposite coatings with enhanced dual active/barrier behavior containing graphene-based carbon hollow spheres as corrosion inhibitor nanoreservoirs, Corros. Sci. 185 (2021), 109428, https://doi.org/10.1016/j.corsci.2021.109428.
[11] S. Zou, X. Xu, Y. Zhu, C. Cao, Microwave-assisted preparation of hollow porous carbon spheres and as anode of lithium-ion batteries, Microporous Mesoporous Mater. 251 (2017) 114–121, https://doi.org/10.1016/j.micromeso.2017.05.062.
[12] X. Hu, K. Shen, C. Han, X. Cao, J. Guo, M. Zhang, Catalytic Mo2C decorated hollow mesoporous carbon spheres as sulfur host for lithium-sulfur batteries with high sulfur loading, J. Solid State Chem. 312 (2022), 123187, https://doi.org/10.1016/j.jssc.2022.123187.
[13] S. Akshatha, S. Sreenivasa, L. Parashuram, V. Udaya kumar, F.A. Alharthi, T.M. Chakrapani Rao, S. kumar, Microwave assisted green synthesis of p-type Co3O4@ Mesoporous carbon spheres for simultaneous degradation of dyes and photocatalytic hydrogen evolution reaction, Mater. Sci. Semicond. Process. 121 (2021), 105432, https://doi.org/10.1016/j.mssp.2020.105432.
[14] H. Liang, G. Wu, H. Zhang, Q. Liu, Q. Yang, S. Xiong, Y. Yue, P. Yuan, Controllable synthesis of N-doped hollow mesoporous carbon with tunable structures for enhanced toluene adsorption, Sep. Purif. Technol. 283 (2022), 120171, https://doi.org/10.1016/j.seppur.2021.120171.
[15] J. Du, A. Chen, L. Liu, B. Li, Y. Zhang, N-doped hollow mesoporous carbon spheres prepared by polybenzoxazines precursor for energy storage, Carbon N. Y. 160 (2020) 265–272, https://doi.org/10.1016/j.carbon.2020.01.018.
[16] J. Du, L. Liu, Y. Yu, Y. Zhang, H. Lv, A. Chen, N-doped ordered mesoporous carbon spheres derived by confined pyrolysis for high supercapacitor performance, J. Mater. Sci. Technol. 35 (2019) 2178–2186, https://doi.org/10.1016/j.jmst.2019.05.029.
[17] S.A. Haddadi, S.A.A. Ramazani, M. Mahdavian, P. Taheri, J.M.C. Mol, Fabrication and characterization of graphene-based carbon hollow spheres for encapsulation of organic corrosion inhibitors, Chem. Eng. J. 352 (2018) 909–922, https://doi.org/10.1016/j.cej.2018.06.063.
[18] R. Behgam, M. Mahdavian, A. Ramazani, Fabrication of hollow carbon spheres doped with zinc cations to enhance corrosion protection of organosilane coatings, Surf. Interfaces 21 (2020), 100696, https://doi.org/10.1016/j.surfin.2020.100696.
[19] S.A. Haddadi, S.A. A. Ramazani, M. Mahdavian, P. Taheri, J.M.C. Mol, Y. Gonzalez-Garcia, Self-healing epoxy nanocomposite coatings based on dual-encapsulation of nano-carbon hollow spheres with film-forming resin and curing agent, Compos. B Eng. 175 (2019), 107087, https://doi.org/10.1016/j.compositesb.2019.107087.
[20] S.A. Haddadi, T.B. Kohlan, S. Momeni, S.A. A. Ramazani, M. Mahdavian, Synthesis and application of mesoporous carbon nanospheres containing walnut extract for fabrication of active protective epoxy coatings, Prog. Org. Coat. 133 (2019) 206–219, https://doi.org/10.1016/j.porgcoat.2019.04.046.
[21] S.A. Haddadi, S.A. A. Ramazani, M. Mahdavian, P. Taheri, J.M.C. Mol, Mechanical and corrosion protection properties of a smart composite epoxy coating with dual-encapsulated epoxy/polyamine in carbon nanospheres, Ind. Eng. Chem. Res. 58 (2019) 3033–3046, https://doi.org/10.1021/acs.iecr.8b06306.
[22] Y. Hao, W. Sun, L. Jiang, J. Cui, Y. Zhang, L. Song, Y. Zhang, Self-healing effect of epoxy coating containing mesoporous polyaniline hollow spheres loaded with benzotriazole, Prog. Org. Coat. 159 (2021), 106445, https://doi.org/10.1016/j.porgcoat.2021.106445.
[23] I. Jevremović, M. Singer, S. Nešić, V. Mišković-Stanković, Inhibition properties of self-assembled corrosion inhibitor talloil diethylenetriamine imidazoline for mild steel corrosion in chloride solution saturated with carbon dioxide, Corros. Sci. 77 (2013) 265–272, https://doi.org/10.1016/j.corsci.2013.08.012.
[24] N. Baig, D.S. Chauhan, T.A. Saleh, M.A. Quraishi, Diethylenetriamine functionalized graphene oxide as a novel corrosion inhibitor for mild steel in hydrochloric acid solutions, New J. Chem. 43 (2019) 2328–2337, https://doi.org/10.1039/C8NJ04771E.
[25] N. Ashraf Ismail, A.M. Moussa, R. Kahraman, R.A. Shakoor, Study on the corrosion behavior of polymeric nanocomposite coatings containing halloysite nanotubes loaded with multicomponent inhibitor, Arab. J. Chem. 15 (2022), 104107, https://doi.org/10.1016/j.arabjc.2022.104107.
[26] N.A. Ismail, A. Khan, E. Fayyad, R. Kahraman, A.M. Abdullah, R.A. Shakoor, Self-healing performance of smart polymeric coatings modified with tung oil and linalyl acetate, Polymers (Basel) 13 (2021), https://doi.org/10.3390/polym13101609.
[27] S. Chen, G. Yang, X. Zhao, N. Wang, T. Luo, X. Chen, T. Wu, S. Jiang, P.A. van Aken, S. Qu, T. Li, L. Du, J. Zhang, H. Wang, H. Wang, Hollow mesoporous carbon spheres for high performance symmetrical and aqueous zinc-ion hybrid supercapacitor, Front. Chem. 8 (2020), https://doi.org/10.3389/fchem.2020.00663.
[28] L. Segal, F.V. Eggerton, Infrared spectra of diethylenetriamine and 2-(2-Aminoethylamino)ethanol, Appl. Spectrosc. 15 (1961) 148–150, https://doi.org/10.1366/000370261774426902.
[29] D.G. O'Sullivan, 727. Vibrational frequency correlations in heterocyclic molecules. Part VII. Benzo-1{,}2{,}3-triazoles, J. Chem. Soc. (1960) 3653–3658, https://doi.org/10.1039/JR9600003653.
[30] D. Shen, J. Yang, X. Li, L. Zhou, R. Zhang, W. Li, L. Chen, R. Wang, F. Zhang, D. Zhao, Biphase stratification approach to three-dimensional dendritic biodegradable mesoporous silica nanospheres, Nano Lett. 14 (2014) 923–932, https://doi.org/10.1021/nl404316v.
[31] C. Yuan, X. Liu, M. Jia, Z. Luo, J. Yao, Facile preparation of N- and O-doped hollow carbon spheres derived from poly(o-phenylenediamine) for supercapacitors, J. Mater. Chem. A 3 (2015) 3409–3415, https://doi.org/10.1039/C4TA06411A.
[32] E. Shin, M.-S. Kim, W. Cho, S.H. Oh, Sulfur/graphitic hollow carbon sphere nanocomposite as a cathode material for high-power lithium-sulfur battery, Nanoscale Res. Lett. 8 (2013) 343, https://doi.org/10.1186/1556-276X-8-343.
[33] W. Kukułka, M. Baca, X. Chen, E. Mijowska, From hollow to solid carbon spheres: time-dependent facile synthesis, Nanomaterials. 8 (2018) 861, https://doi.org/10.3390/nano8100861.
[34] G.J. Brug, A.L.G. van den Eeden, M. Sluyters-Rehbach, J.H. Sluyters, The analysis of electrode impedances complicated by the presence of a constant phase element, J. Electroanal. Chem. Interfacial Electrochem. 176 (1984) 275–295, https://doi.org/10.1016/S0022-0728(84)80324-1.
[35] E.P.M. van Westing, G.M. Ferrari, J.H.W. de Wit, The determination of coating performance with impedance measurements-I. Coating polymer properties, Corros. Sci. 34 (1993) 1511–1530, https://doi.org/10.1016/0010-938X(93)90245-C.
[36] S. Habib, A. Hassanein, R. Kahraman, E. Mahdi Ahmed, R.A. Shakoor, Self-healing behavior of epoxy-based double-layer nanocomposite coatings modified with Zirconia nanoparticles, Mater. Des. 207 (2021), 109839, https://doi.org/10.1016/j.matdes.2021.109839.
[37] M. Benoit, C. Bataillon, B. Gwinner, F. Miserque, M.E. Orazem, C.M. Sánchez-Sánchez, B. Tribollet, V. Vivier, Comparison of different methods for measuring the passive film thickness on metals, Electrochim. Acta 201 (2016) 340–347, https://doi.org/10.1016/j.electacta.2015.12.173.
[38] X. Cao, F. Huang, C. Huang, J. Liu, Y.F. Cheng, Preparation of graphene nanoplate added zinc-rich epoxy coatings for enhanced sacrificial anode-based corrosion protection, Corros. Sci. 159 (2019), 108120, https://doi.org/10.1016/j.corsci.2019.108120.
[39] M. Mahdavian, M.M. Attar, Another approach in analysis of paint coatings with EIS measurement: phase angle at high frequencies, Corros. Sci. 48 (2006) 4152–4157, https://doi.org/10.1016/j.corsci.2006.03.012.
[40] Y. Zuo, R. Pang, W. Li, J.P. Xiong, Y.M. Tang, The evaluation of coating performance by the variations of phase angles in middle and high frequency domains of EIS, Corros. Sci. 50 (2008) 3322–3328, https://doi.org/10.1016/j.corsci.2008.08.049.
[41] H.H. Hassan, E. Abdelghani, M.A. Amin, Inhibition of mild steel corrosion in hydrochloric acid solution by triazole derivatives: part I. Polarization and EIS studies, Electrochim. Acta 52 (2007) 6359–6366, https://doi.org/10.1016/j.electacta.2007.04.046.
[42] Q. Li, Z. Feng, L. Liu, H. Xu, W. Ge, F. Li, M. An, Deciphering the formation mechanism of a protective corrosion product layer from electrochemical and natural corrosion behaviors of a nanocrystalline zinc coating, RSC Adv. 5 (2015) 32479–32490, https://doi.org/10.1039/C5RA02777B.
[43] M.H. Sliem, M. Afifi, A. Bahgat Radwan, E.M. Fayyad, M.F. Shibl, F.E.-T. Heakal, A. M. Abdullah, AEO7 surfactant as an eco-friendly corrosion inhibitor for carbon steel in HCl solution, Sci. Rep. 9 (2019) 2319, https://doi.org/10.1038/s41598-018-37254-7.
[44] M. Nawaz, R.A. Shakoor, R. Kahraman, M.F. Montemor, Cerium oxide loaded with Gum Arabic as environmentally friendly anti-corrosion additive for protection of coated steel, Mater. Des. 198 (2021), 109361, https://doi.org/10.1016/j.matdes.2020.109361.